An Online Peak Shaving Controller for Optimized Power-electronic Converter Lifetimes in Turbine Array Generation Systems

Alastair P. Thurlbeck, *Student Member, IEEE,* and Yue Cao, *Senior Member, IEEE*

***Abstract*—Wind and hydrokinetic turbines play an essential role in the transition to carbon-free electricity generation, and improving the economics of turbine systems can accelerate this change. Recognizing that operational costs represent a significant share of the total generation costs, researchers have proposed methods for optimizing the turbine system maintenance while considering the impact of power-electronic converter lifetime on the maintenance costs. This work considers how peak-shaving can be applied to turbine units across an array to exchange energy generation for prolonged power-electronic converter lifetimes and reduced maintenance visits. This work proposes an online peak shaving controller (PSC) that finds the optimal peak-shaving actions by minimizing a function of the predicted levelized cost of energy (LCOE). This real-time minimization of LCOE via a model predictive control style framework ensures the PSC is economically beneficial to the system. The PSC simulates the turbine system with different peak-shaving actions over a prediction horizon, then calculates LCOE considering the power-electronic converter lifetimes and turbine array energy generation. A hardware test demonstrates the real-time peak-shaving action leveraged by the PSC, while a simulation case study for a wind turbine array demonstrates the economic benefit offered over the array's full lifecycle.**

***Index Terms*—Turbines, Wind energy, Hydrokinetic energy, Power conversion, Power electronics, Predictive maintenance, Remaining life assessment, Condition monitoring, Model predictive control, LCOE.**

I. Introduction

Wind turbines are a well-established and rapidly growing source of renewable energy. In 2020, wind turbines accounted for 8.3% of electricity generation in the USA and the largest share of new electricity generation capacity additions [1]. In contrast to wind turbines, the commercial deployment of hydrokinetic turbine (HKT) systems - submerged turbines that capture the kinetic energy of flowing water - remains limited, primarily due to the high cost. However, researchers suggest that leveraging hydrokinetic energy generation is necessary to accelerate the transition toward increased renewable energy generation and reduced carbon emissions [2].

Metrics such as levelized cost of energy (LCOE) can quantify the economic performance of wind and hydrokinetic turbine projects. In simple terms, LCOE is the ratio of costs to energy generation. Costs comprise the capital expenditures (CapEx) and operational expenditures (OpEx), with operations and maintenance (O&M) costs comprising a significant share of OpEx. Literature surveying large wind turbine systems suggests that O&M costs account for 25-34% of the total lifecycle costs [3], [4]. Further, researchers suggest that as wind turbine system LCOE continues to fall, O&M and OpEx costs will be responsible for an increasing share of the LCOE [5]–[7]. Therefore, exploring advanced techniques to reduce O&M costs or prolong plant lifespan is essential to further reducing turbine system LCOE. While literature on the operating costs of HKTs is limited, [8] provides baseline CapEx and OpEx for ocean wave power devices, from which OpEx accounts for around 43-56% of the total lifecycle costs over a 20-year lifespan.

Power electronics, especially in the direct-drive powertrain, plays a major role in wind and HKT generation. The maintenance strategy of the power-electronic (PE) system and the rest of the turbine system has a significant impact on O&M costs [9]. Considering this, researchers have proposed various numerical techniques for finding the optimal maintenance strategy for multi-component systems such as wind turbines. An optimal maintenance strategy is typically found by minimizing an objective function composed of the costs or risks associated with maintenance actions and component failures [10]–[13]. These works consider various combinations of preemptive, condition-based, and corrective maintenance actions in searching for the optimal maintenance strategy. Additionally, these techniques consider how multiple maintenance actions can be performed concurrently in a single maintenance visit according to group-based or opportunistic maintenance policies.

An array of wind or hydrokinetic turbines presents a challenging maintenance optimization problem since the array comprises numerous turbine units, each of which is a complex multi-component system. Further, each turbine unit may age and degrade at a different rate. Ref [11] presents a maintenance optimization framework for an array of offshore wind turbines, while [13] demonstrates the advantage of a group maintenance policy for the same application. However, while these techniques are effective in identifying an optimal maintenance strategy, they do not consider how the operation of the turbine system, especially regarding the PE system, can be modified to further improve the turbine system's economic performance.

Recently, [14] proposed a health-orientated power control strategy for a direct-drive wind turbine. A receding horizon predictive controller maximizes the turbine system economic

This work was supported in part by the U.S. Department of Energy Advanced Research Projects Agency-Energy (ARPA-E) Award under Grant DE-AR0001438.

A. P. Thurlbeck and Y. Cao are with the School of Electrical Engineering and Computer Science, Oregon State University, Corvallis, OR 97331, USA. e-mail: thurlbea@oregonstate.edu, yue.cao@oregonstate.edu.

revenue by flattening the temperature variation of the PE converter switching devices. While effective, the proposed controller considers a single turbine unit in isolation. In a turbine array employing a group maintenance strategy, the economics of applying power control to a single unit is intertwined with the state of all other turbine units across the array. Therefore, a more complex strategy or controller is required to consider this interplay between the turbines.

Aside from [14], the concept of exchanging energy generation for prolonged PE converter lifetimes is not explored in the literature, and no prior work has explored how this concept can be implemented in a turbine array system employing group maintenance policies across the array. Therefore, this paper proposes a peak shaving controller (PSC) in which the rated power of each turbine unit, with consideration of the array system, is altered on-the-fly during operation, cutting off some peaks in the wind or water profile. In doing so, the PSC prolongs some PE converter lifetimes at the expense of energy generation. To consider this trade-off, as well as the intertwined economics of the array due to the group maintenance policy, the PSC minimizes an LCOE function for the entire array within a model predictive control style framework, thereby determining the optimal peak-shaving action for each individual turbine unit.

This work comprises three contributions to the literature: Firstly, the concept of leveraging power-control actions to improve system economics explored in [14] is expanded to a turbine array system with group maintenance policies. Secondly, derating each turbine unit's rated power on-the-fly is explored as a means to implement peak-shaving actions for both variable- and fixed-pitch turbine designs. Thirdly, real-time online minimization of system LCOE is used to set the power-control actions, ensuring maximum economic performance.

This paper is organized as follows. Section II introduces the turbine array system, detailing its operation, modeling, and control. Section III describes the maintenance strategy applied to the turbine array PE converters. Section IV uses simulation and experimental testing to investigate and demonstrate the peak-shaving concept. Section V details the proposed PSC. Section VI uses a simulation case study for a wind turbine array to explore the efficacy of the PSC. Finally, Section VII summarizes the contributions and concludes this paper.

II. Turbine System Operation and Modeling

The proposed PSC simulates the entire turbine system over a prediction horizon, which requires detailed multi-physics modeling. Therefore, this section describes the operation and modeling of the turbine system, considering mechanical, electrical, thermal, and aging behaviors. Additionally, these models are used to investigate the peak-shaving concept in Section IV and demonstrate PSC performance in the Section VI case study. Averaged steady-state models are used to accurately capture turbine system power generation and PE converter aging over a long-timespan mission profile simulation. Fast-timescale dynamics such as PWM switching, blade-pitch actuation, and transient behaviors are beyond the paper's scope; however, the thermal models include the dynamic behavior associated with the cooling system's heat capacity.

A. Turbine System Overview

Fig. 1. shows an overview of a direct-drive turbine array applicable to wind and hydrokinetic systems. The array has n turbine units with each comprising a turbine, permanent magnet synchronous generator (PMSG), and a back-to-back AC-DC-AC PE converter system with an LCL filter. The PE system allows for variable-speed operation of the turbine while controlling real and reactive power flow to the grid. The proposed PSC, explained in detail in Section V, alters the rated turbine powers on-the-fly to the optimal values $Prated_{opt}$. Note that the PSC does not replace the existing controls within each turbine unit. The PSC inputs are the wind or water velocity forecast, the system's economic parameters, the turbine unit generated powers P_n, and the junction temperatures of the converter switching devices T_J.

B. Turbine System Modeling

While the example systems are both variable-speed, the wind-turbine system is variable-pitch and the HKT system is fixed-pitch. Below their rated power, both designs allow for maximum power extraction. However, when rated power is reached at higher wind or water speeds, their respective methods of power limiting are different, affecting the applicability of the proposed PSC. Turbine operation in these regions is detailed below for both systems.

1) Operation below rated power: The turbine does not operate when below the turbine cut-in speed u_{ci}. Otherwise, the turbine is behavior is as follows. The power of the wind or water through the swept area of the turbine is given by

$$P_{fluid} = \frac{1}{2}\rho\pi r^2 u^3 \tag{1}$$

where ρ is the air or water density, r is the turbine blade radius, and u is the air or water velocity. The generator speed is controlled to achieve the optimal tip-speed ratio λ_{opt}, corresponding to the maximum power coefficient $C_{P(max)}$ and maximum power extraction. Thus turbine power, speed, and torque are calculated as

$$P_r = C_{P(max)} P_{fluid} \qquad w_r = \frac{\lambda_{opt} u}{r} \qquad T_r = \frac{P_r}{w_r} \tag{2}$$

2) Operation at rated power: The power limiting behavior differs between the fixed- and variable-pitch turbine designs [15], [16]. In the variable-pitch control case, when the turbine rated power is reached, turbine speed is held constant and the turbine blade pitch is controlled to intentionally reduce C_P. Since the turbine pitching does not affect the rest of the electrical system, it does not need to be modeled in detail. Turbine power, speed, and torque are calculated as

$$P_r = P_{rated} \qquad w = w_{r(max)} \qquad T_r = \frac{P_r}{w_r} \tag{3}$$

where P_{rated} is the turbine rated power, and $w_{r(max)}$ is the turbine speed corresponding to the turbine entering the power-limited region.

In the fixed-pitch case, assisted stall regulation is used. When the turbine rated power is reached, turbine speed is

reduced to induce the stall condition, thereby limiting the power that is extracted from the wind or water. Turbine power, speed, and torque are calculated as

$$P_r = P_{rated} \qquad w_r = \frac{\lambda(C_P)u}{r} \qquad T_r = \frac{P_r}{w_r} \tag{4}$$

where $\lambda(C_P)$ is the tip-speed-ratio obtained from a lookup table of the turbine's C_P curve. The required C_P is given by $C_P = P_{rated}/P_{fluid}$.

At very high wind or water speeds, the turbine will cease operation when it reaches the cut-out speed u_{co}.

C. PMSG Modeling

By regulating the PMSG torque, the PMSG speed can be controlled to achieve the desired turbine speed. The calculated turbine speed and torque and DC bus voltage V_{dc} are passed to the PMSG model. In steady-state, 5% core and mechanical losses are assumed, thus the electromagnetic torque is calculated as $T_{em} = 0.95T_r$.

The PMSG modeling and control use the d-q rotating reference frame aligned to the permanent-magnet rotor flux. Therefore assuming zero field weakening, the d-q axis currents and rms phase currents are given by

$$i_d = 0 \qquad i_q = \frac{2T_{em}}{3pp\lambda_{fd}} \qquad I_{ph} = \frac{i_q}{\sqrt{2}} \tag{5}$$

where pp is the number of pole pairs and λ_{fd} is the rotor flux linkage. The PMSG power generated to the gen-side converter, after subtracting losses, is calculated by

$$P_{loss(gen)} = 3I_{ph}^2 R_s + 0.05T_r w_r \tag{6}$$

$$P_{gen} = T_r w_r - P_{loss(gen)} \tag{7}$$

where R_s is the stator resistance. The d-q voltages are

$$V_d = R_s i_d - w_e L_q i_q \tag{8}$$

$$V_q = R_s i_q + w_e(\lambda_{fd} + L_d i_d) \tag{9}$$

where L_d and L_q are the stator d and q axis inductances, respectively. w_e is the electrical frequency, calculated as $w_e = pp \cdot w_r$. Then the rms phase voltage, and the phase angle ψ between the voltage and current are given by

$$V_{ph} = \frac{\sqrt{V_d^2 + V_q^2}}{\sqrt{2}} \qquad \psi = \tan^{-1}(\frac{V_q}{V_d}) - \frac{\pi}{2} \tag{10}$$

Finally, the maximum modulation index is calculated as $M_{max} = 2\sqrt{2}V_{ph}/V_{dc}$.

D. Gen-side PE Converter Modeling

The PMSG phase currents, phase voltages, phase angle, and modulation index are passed onto the gen-side converter model. Since the goal of the proposed PSC is to prolong converter lifetime, the gen-side converter requires an electrical system averaged model, a thermal model, and a lifetime model. The gen-side converter electrical model is described in this subsection, followed by the grid-side converter and LCL electrical model in the next. Then the PE converter thermal and lifetime modeling common to both the gen-side and grid-side converters will follow.

IGBT conduction and switching losses as well as diode reverse recovery losses are calculated according to [17]. The method first calculates voltage rise and fall times considering the switching voltages and currents, gate-drive, device capacitance, and miller plateau effect. The required average and rms IGBT and diode currents are calculated using equations from [18].

The losses in the DC bus capacitor are calculated as $P_{Cdc} = I_{C(rms)}^2 ESR$, where $I_{C(rms)}$ is calculated using equation from [18] and ESR is the capacitor equivalent series resistance. Similarly, wire conduction losses are calculated for the phase-lines between the PMSG and the gen-side converter. Then the total converter losses and power generated to the DC bus are given by

$$P_{loss(genside)} = P_{IGBTs} + P_{diodes} + P_{Cdc} + P_{wiring} \tag{11}$$

$$P_{DC} = P_{gen} - P_{loss(genside)} \tag{12}$$

where P_{Cdc} and P_{wiring} are the conduction losses in the DC bus capacitor and wires to the PMSG.

E. Grid-side PE Converter & LCL Filter Modeling

The grid-side converter is modeled similarly to the gen-side converter. However, the grid-side converter is connected to the 3ph AC grid via an LCL filter with passive damping, and the LCL filter model is solved in tandem with the grid-side converter model.

The inputs to the model are the power supplied to the DC bus by the gen-side converter, the DC bus voltage, and the grid voltage and frequency. The combined converter and filter model is solved iteratively, since at first the power loss is unknown, yet the real power supplied to the grid is required to solve the system of equations. An initial guess is that grid power is $P_g = P_{DC}$. The LCL filter has converter-side inductance and associated resistance L_{f1} and R_{f1}, grid-side inductance and associated resistance L_{f2} and R_{f2}, capacitance

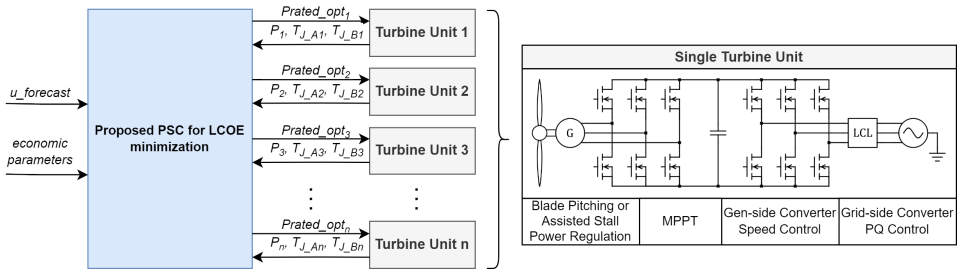

Fig. 1. Overview of a direct-drive turbine array with the proposed PSC.

This article has been accepted for publication in IEEE Transactions on Energy Conversion. This is the author's version which has not been fully edited and content may change prior to final publication. Citation information: DOI 10.1109/TEC.2022.3231286

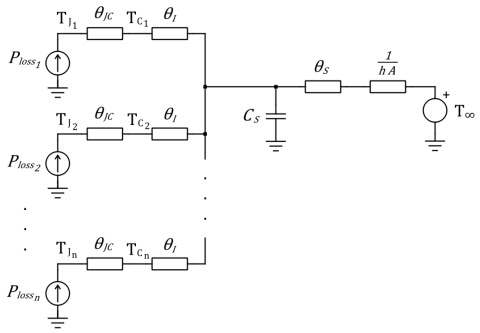

Fig. 2. Thermal-equivalent circuit model for the gen-side and grid-side converters.

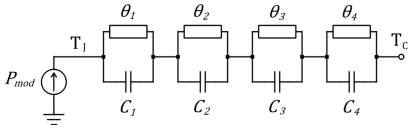

Fig. 3. 4-RC thermal-equivalent circuit model for the device junction-case thermal impedance.

C_f and damping resistance R_f. The d-q axis grid currents are calculated as

$$i_{g(d)} = \frac{2P_g}{3V_{g(d)}} \qquad i_{g(q)} = -\frac{2Q_{ref}}{3V_{g(q)}} \tag{13}$$

where $V_{g(dq)}$ are the d-q axis grid voltages. Then the d-q axis voltages at the central node of the LCL filter are given by

$$V_{x(d)} = V_{g(d)} + R_{f2}i_{g(d)} - w_g L_{f2} i_{g(q)} \tag{14}$$
$$V_{x(q)} = V_{g(q)} + R_{f2}i_{g(q)} + w_g L_{f2} i_{g(d)} \tag{15}$$

Then the d-q axis capacitor currents are given by

$$i_{c(d)} = -C_f^2 R_f^2 w_g^2 (i_{g(d)} + \frac{V_{x(q)}/R_f - C_f V_{x(d)} w_g)}{C_f R_f w_g}) \tag{16}$$

$$i_{c(q)} = -C_f^2 R_f^2 w_g^2 (i_{g(q)} - \frac{V_{x(d)}/R_f + C_f V_{x(q)} w_g}{C_f R_f w_g}) \tag{17}$$

Then the converter d-q output currents are calculated as

$$i_{f(d)} = i_{g(d)} + i_{c(d)} \qquad i_{f(q)} = i_{g(q)} + i_{c(q)} \tag{18}$$

Then the converter d-q output voltages are found by

$$v_{f(d)} = V_{x(d)} + R_{f1}i_{f(d)} - w_g L_{f1} i_{f(q)} \tag{19}$$
$$v_{f(q)} = V_{x(q)} + R_{f1}i_{f(q)} + w_g L_{f1} i_{f(d)} \tag{20}$$

The rest of the model proceeds similarly to that of the gen-side converter model, with $i_{f(dq)}$ and $V_{f(dq)}$ used to calculate the converter's rms current and voltage, and the phase angle between them. The power loss is found as before, albeit now with the addition of the conduction losses in the LCL filter resistances. The real-power to the grid is then given by

$$P_g = P_{DC} - P_{loss(gridside)} \tag{21}$$

The model iterates k times until the following stopping criterion is met

$$|P_g(k) - P_g(k-1)| \leq 1 \times 10^{-3} \tag{22}$$

F. PE Converter Thermal Modeling

IGBT junction and case temperatures are calculated using the thermal equivalent circuit of Fig. 2. P_{loss} are the IGBT power losses calculated by the above electrical model. T_J are the device junction temperatures, T_C are the device case temperatures, h is the convective heat transfer coefficient, and A is the heatsink surface area. T_∞ is the wind or water temperature beyond the thermal boundary layer. θ_{JC}, θ_I, and θ_S are the junction-case, interface, and heatsink thermal resistances, respectively. Note that θ_S represents the conductive heat transfer across the heatsink material, whereas $1/(hA)$ represents the convective heat transfer from the heatsink surface to the wind or water. A rainflow algorithm [19] then performs thermal cycle counting to obtain the low-frequency junction and case thermal cycles for use with the lifetime models.

The lifetime models also require the number and magnitude of fundamental-frequency junction temperature cycles. Fundamental-frequency thermal cycles are calculated using a 4-RC model of the junction-case thermal impedance, shown in Fig. 3, using the mathematical method from [20]. P_{mod} is an approximation of instantaneous device power loss which varies over the fundamental period. θ and C values are the thermal resistances and capacitance's of the 4RC junction-case thermal impedance model, and are obtained from the device datasheet [21].

G. PE Converter Lifetime Modeling

Lifetime modeling estimates the gen-side and grid-side converter life consumption (LC), allowing implementation of the CBM strategy and providing the necessary aging information for the proposed peak-shaving controller. This work assumes that the IGBTs dominate the PE converter aging and that the IGBTs in a single gen-side or grid-side converter age concurrently. Therefore, lifetime models of a single gen-side and grid-side IGBT constitute the lifetime models of the respective PE converters.

IGBT aging is driven by thermal cycling of the IGBT junction and case. The lifetime models consider the fundamental-frequency (e.g., 60 Hz for the grid-side) thermal cycling caused by the sinusoidal AC currents and the low-frequency thermal cycling caused by the variation of the load and average power. The high-frequency thermal cycling due to the PWM switching is not included since the magnitude of cycles at the PWM frequency is negligible. The "physics-of-failure" (PoF) approach to lifetime modeling is used [22], [23], in which the individual physical failure mechanisms of the IGBT chip and packaging are considered independently.

This work constructs PoF lifetime models using accelerated life test data for HiPak IGBT modules [24]. The simulated turbine systems in this work consider discrete IGBTs rather than IGBT modules; however, the failure modes are expected to be similar. Therefore, although the lifetime models do not offer absolute accuracy, they do facilitate relative comparisons and study of the PSC relative to a baseline system.

The life test data gives the B_{10} lifetime, which is defined as when 10% of the population is expected to have failed, as a function of absolute temperature, thermal cycle magnitude, and thermal cycle time. Three physical failure mech-

anisms are considered: conductor lead and substrate solder joint degradation, chip solder joint degradation, and bond wire degradation. Conductor lead and substrate solder joint degradation is packaging related and dependent on the case temperature. Hence, only low-frequency thermal cycles are considered, since the heat-capacity of the case smooths out the fundamental-frequency junction temperature variations. On the other hand, the chip solder joint and bond-wire degradations are chip related and dependent on device junction temperature. Thus both fundamental-frequency and low-frequency thermal cycles are considered.

For each of these three physical failure mechanisms, a Palmgren-miner damage accumulation model is used to find the B_{10} LC as:

$$LC = \sum_{i=1}^{k} \frac{n_i}{N_{fi}} \tag{23}$$

where n_i is the number of cycles experienced at the ith cycle magnitude, and N_{fi} is the number of cycles to the B_{10} lifetime at the ith cycle magnitude. The linear damage accumulation model is valid for summing up the damage due to thermal cycles of different magnitudes, as well as summing together the damage from fundamental-frequency and low-frequency thermal cycles [20], [25]. In PoF lifetime modeling, the overall B_{10} LC of the IGBT is then given by the maximum of the above three individual failure mechanism LCs:

$$LC_{IGBT} = max(LC_{pak}, LC_{chip-s}, LC_{chip-bw}). \tag{24}$$

III. Turbine Array Maintenance Strategy

As explained earlier, this paper mainly focuses on the maintenance requirements of the PE converters. The PE converters use a group and condition-based maintenance strategy, based on the B_{10} LCs of the PE converters. The maintenance strategy is explained below for the gen-side converters, though an identical strategy is applied separately to the grid-side converters. Note that the maintenance strategies of the gen-side and grid-side converters are independent of one another.

The gen-side PE converter B_{10} LCs are monitored across the array. The maintenance threshold is set at $LC = 1$, which corresponds to the B_{10} lifetime. When the first converter reaches the threshold, a group maintenance visit is scheduled. During this visit, all the gen-side converters across the array are replaced, and their B_{10} LCs reset to zero. This group CBM strategy prevents the power control strategy of [14] from being easily extended to an array of turbines since the timing of maintenance depends only on the gen-side and grid-side converters with the highest LC. i.e., exchanging energy generation for prolonged converter lifetimes offers no benefit if the turbine unit's gen-side or grid-side LC is not the highest in the array.

Critically, while the turbine systems across the array are considered to be physically and electrically independent of one another, this group maintenance strategy means that they are economically intertwined. i.e., to determine if peak-shaving should be applied to any single turbine in the array requires simultaneous consideration of every other turbine in the array.

TABLE I
Turbine System Parameters

Parameter	Wind-turbine System	HKT System
Power Limit Control	Blade-pitching (feathering)	Assisted stall regulation
Rated Power	24.0 kW	32.2 kW
Turbine $C_{p(max)}$	0.45	0.45
Turbine Radius	1.88 m	0.73 m
PMSG	Alxion 400STK4M-800	Alxion 800STK1M-400
PE Conv. IGBTs	Infineon IKW20N60T	Infineon IKW20N60T
PE. Conv. f_{sw}	10 kHz	10 kHz
DC Bus Voltage	450 VDC	600 VDC
Grid Bus Voltage	230 VAC	230 VAC

TABLE II
Cooling System Parameters

Parameter	Wind-turbine System	HKT System
θ_{JC}	0.9 K/W	0.9 K/W
θ_I	0.333 K/W	0.333 K/W
θ_S	6.63 mK/W	33.2 mK/W
C_s	0.731 kJ/K	3.66 kJ/K
A	0.165 m^2	0.165 m^2

IV. Turbine System Behavior with Peak-shaving

A. Simulated Peak-shaving Behavior

In this subsection, idealized wind and water velocity waveforms are used to 1) investigate the applicability of the peak-shaving concept to the variable- and fixed-pitch turbine designs, and 2) demonstrate the impact to the electrical system when peak-shaving is applied. Here two example systems are used: A variable-speed variable-pitch wind turbine system; and a variable-speed fixed-pitch HKT system. The parameters of these two systems are shown in Table I. Additionally, parameters of the PE converter cooling systems are given in Table II.

1) Variable-speed variable-pitch wind turbine: Fig 4. shows the response of the simulated variable-pitch wind turbine system to an idealized wind velocity waveform over a 24 hr simulation period. The base rated power of this turbine system is 24 kW. When peak-shaving is applied, the rated power of the turbine system is artificially reduced or derated, to "shave" the peak of the power curve. Fig. 4 includes two cases of peak shaving at 21.6 and 19.2 kW. Fig. 4(a) shows the turbine power against the wind velocity, indicating the power peak-shaving effect. Fig. 4(b) shows the turbine speed and torque corresponding to the turbine powers and wind speed of Fig. 4(a). When the power is limited, the speed and torque are constant due to blade-pitch control. Fig. 4(c) shows the IGBT junction temperatures in the gen-side and grid-side PE converters. When the turbine power is limited, there is a reduction in the peak junction temperatures in both converters. Considering this 24 hr period as a single thermal cycle, the magnitude of the device thermal cycles is reduced, meaning the IGBTs have degraded slightly less in the power limited case.

Fig. 4(c) also shows two interesting behaviors. Firstly, the temperatures dip downwards during the power-limited period. This is due to the wind speed continuing to increase, result-

This article has been accepted for publication in IEEE Transactions on Energy Conversion. This is the author's version which has not been fully edited and content may change prior to final publication. Citation information: DOI 10.1109/TEC.2022.3231286

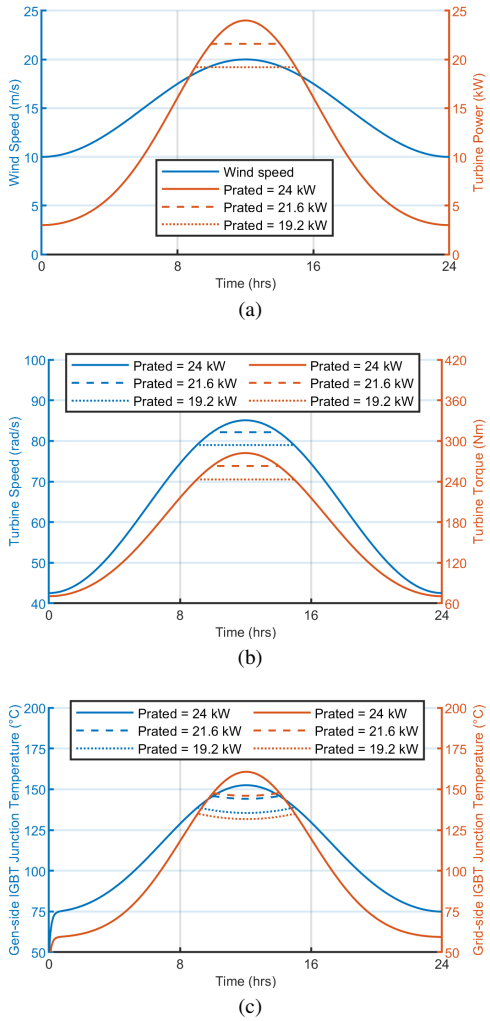

Fig. 4. Simulation of a variable-speed variable-pitch wind turbine with reducing rated power. (a) Wind speed and turbine power. (b) Turbine rotational speed and torque. (c) Gen-side and grid-side PE converter IGBT junction temperatures.

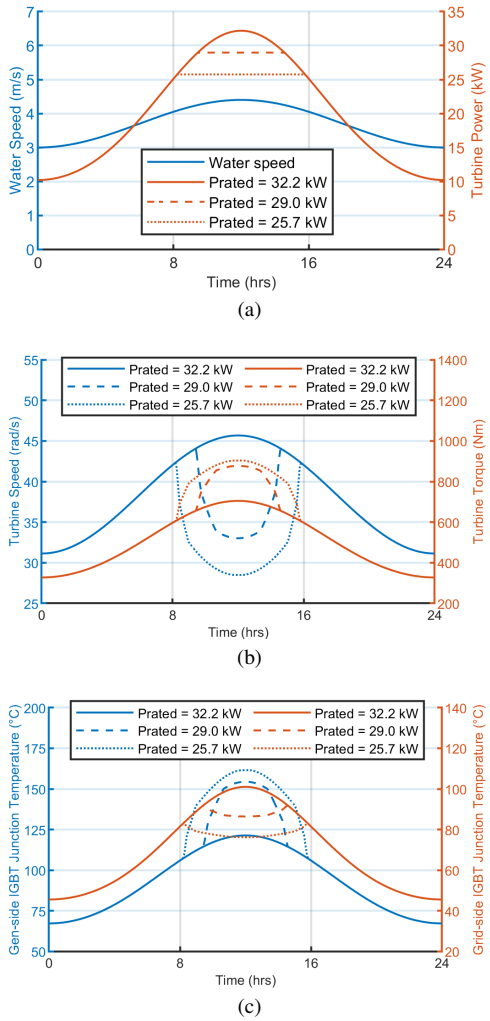

Fig. 5. Simulation of a variable-speed, fixed-pitch HKT with reducing rated power. (a) Water speed and turbine power. (b) Turbine rotational speed and torque. (c) Gen-side and grid-side PE converter IGBT junction temperatures.

ing in peak convective-cooling at t = 12 hrs. Secondly, the temperature reductions are smaller in the gen-side converter compared to the grid-side converter. This is because the IGBT losses are dominated by conduction losses in this case. When the power is limited, both turbine speed and torque are lower. Therefore, generator speed and current are lower. In the gen-side converter, this means the reduced power corresponds to lower voltages and currents. Whereas in the grid-side converter, the DC bus and grid voltages are fixed. Hence the reduced power corresponds to lower current only. Therefore, the effect of reduced conduction losses is more prominent in the grid-side converter.

Since the magnitude of thermal cycles can be reduced in both the gen-side and grid-side converters, the variable-pitch wind turbine system is an ideal candidate for application of the proposed peak-shaving controller.

2) Variable-speed fixed-pitch HKT: Fig. 5 shows the results for the simulated fixed-pitch HKT system. Fig. 5(a) shows similar behavior to Fig. 4(a), with reduced rated powers leading to limited turbine power. However, fixed-pitch HKT uses assisted stall regulation to limit the power. As Fig. 5(b) shows, the turbine speed is reduced to induce the stall condition. However, the turbine torque is then increased to maintain the turbine power at a constant value. Fig. 5(c) shows the effect on the gen-side and grid-side PE converter IGBT junction temperatures. At reduced rated power, the increased torque corresponds to higher gen-side converter currents. Since the conduction losses dominate, the gen-side temperatures are significantly increased, and the magnitude of the thermal cycles here is increased. In the grid-side converter, the reduced power results in lower currents, losses, and junction temperatures, since the DC bus voltage and grid voltage are fixed. While the peak-shaving has the intended effect on the grid-side converter, it actually accelerates the degradation and aging of the gen-side converter. Therefore, the fixed-pitch HKT is not an ideal candidate system for the peak-shaving controller.

B. Experimental Peak Shaving Demonstration

A small-scale test platform shown in Fig. 6 demonstrates the peak-shaving control for the variable-speed, variable-pitch wind turbine design. A ”dyno” motor controlled by a 3-phase inverter and a TI development board emulates the turbine behavior. The dyno controller regulates the dyno motor torque according to wind speed and generator shaft speed. A

This article has been accepted for publication in IEEE Transactions on Energy Conversion. This is the author's version which has not been fully edited and content may change prior to final publication. Citation information: DOI 10.1109/TEC.2022.3231286

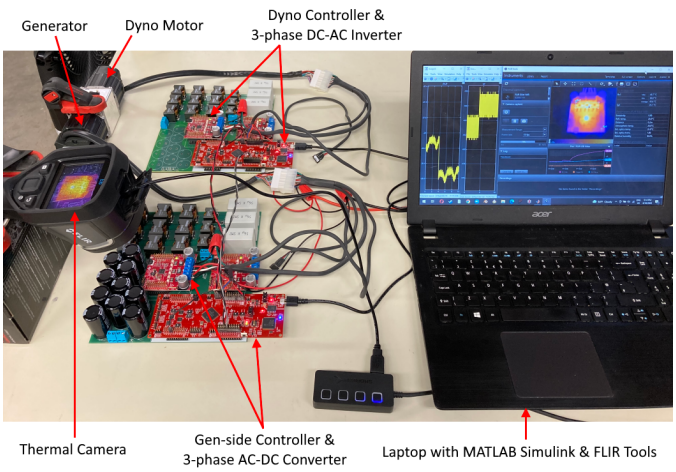

Fig. 6. Small-scale hardware test platform for peak-shaving demonstration.

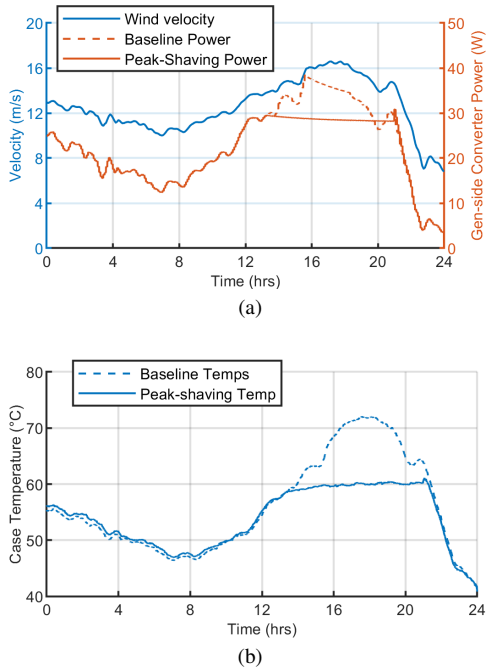

Fig. 7. Experimental demonstration of an example peak-shaving action. (a) Wind speed and gen-side converter power generation. (b) Gen-side converter MOSFET case temperature.

lookup table is used for turbine C_P, where the tip-speed-ratio and blade pitch are the inputs. The dyno motor is coupled directly to the generator. A 3-phase AC-DC converter (the gen-side converter), controlled by a second TI development board, connects the generator to the DC bus. The gen-side controller regulates the generator speed to achieve the optimal tip-speed-ratio throughout the dyno emulated wind profile. Without loss of generality, this subsection considers only the gen-side converter. The hardware test uses MOSFETs given the lab-scale power levels; however, the control behavior and temperature trends are expected to be similar to that of IGBTs, which are used at the simulation level in the rest of the paper.

A thermal camera captures the MOSFET case temperatures, which is sufficient to observe the general effect of the peak-shaving behavior on PE converter temperatures. Note that the

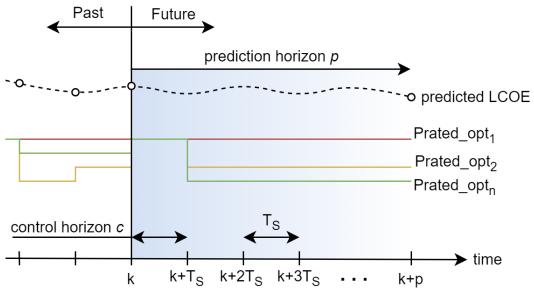

Fig. 8. Timing of the proposed PSC process.

PE converters considered in simulation in the rest of this paper use IGBTs, and both junction and case temperatures are required for the lifetime modeling. In real deployment of the PSC, junction temperature can be estimated by measuring the case temperature with a thermocouple, and calculating junction temperature as $T_J = T_C + P_{loss}\theta_{JC}$.

Fig. 7 shows an example peak-shaving action applied to the experimental platform. The peak-shaving action comprises a dynamically adjusted turbine rated power (artificial derating of the turbine on-the-fly). This adjustable turbine rated power is the output of the proposed PSC. The hardware test uses 24 hrs of scaled wind data from [26], and the test is performed 20x faster than real-time. Fig. 7(a) shows the wind velocity and the measured gen-side PE converter power (generated to the DC bus). When the peak-shaving action is applied, the peak power generation is reduced from 38 to 30 W. Fig. 7(b) shows the measured MOSFET case temperatures. Due to the reduced device losses associated with the lower power generation, the peak case temperature is reduced from 72°C to 61°C, corresponding to a reduced low-frequency thermal cycle magnitude. Considering this test period in isolation, the peak-shaving action reduces the measured energy generation by 13.5%, while the gen-side converter LC is 17.1% lower.

This hardware test shows how a single peak-shaving action can realize prolonged PE converter lifetimes at the expense of energy generation. However, it is important to understand the cumulative effect of numerous peak-shaving actions over the lifespan of the turbine array system on the LCOE. For this purpose, the simulation case study in Section VI will demonstrate PSC performance over longer timescales.

V. Proposed Online Peak Shaving Controller for LCOE Minimization

The previous section has shown how a peak-shaving action can exchange energy generation for slowed PE converter aging. Even with just a single turbine it is challenging to determine the most economically beneficial peak-shaving actions over the turbine's lifecycle. Now consider the case of a turbine array with the group and condition-based maintenance strategy described in Section III. The economic impact of applying peak-shaving to a single turbine unit cannot be determined without considering the state of every other turbine unit, since the timing and costs of maintenance visits are dependent on the turbine unit PE converters which first reach their B_{10} lifetime. Instead, all turbines must be considered concurrently. To solve this problem, the PSC is proposed in detail in this section.

This article has been accepted for publication in IEEE Transactions on Energy Conversion. This is the author's version which has not been fully edited and content may change prior to final publication. Citation information: DOI 10.1109/TEC.2022.3231286

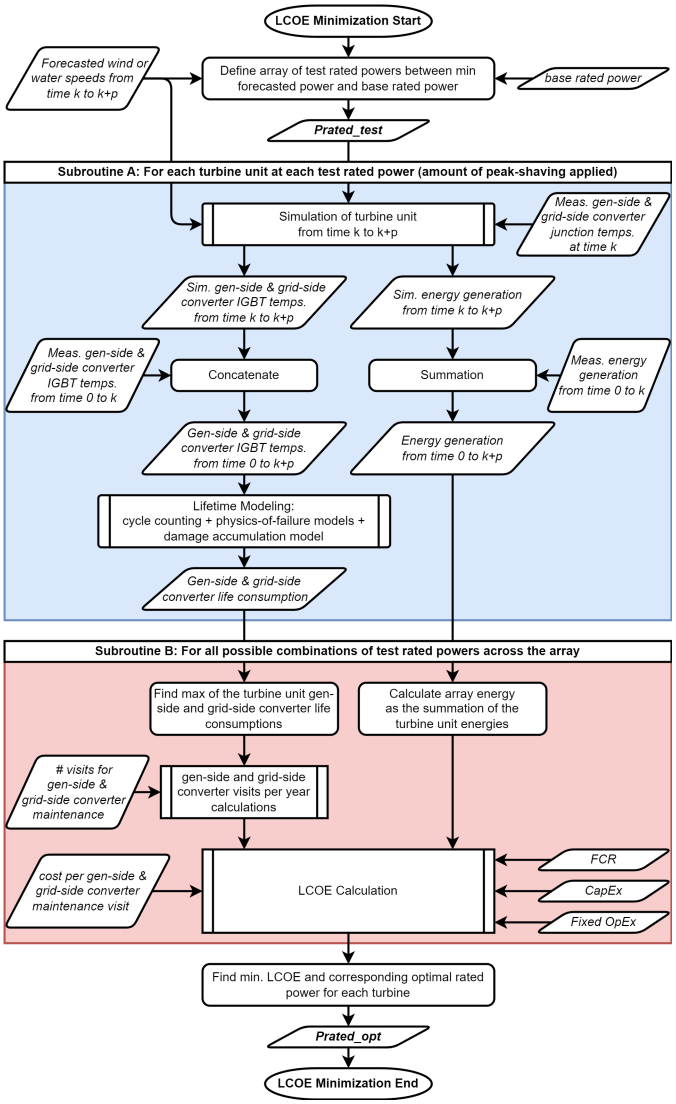

Fig. 9. Flowchart of proposed PSC process.

The proposed PSC uses a model predictive control (MPC) style framework. Note that the PSC process operates over a slow timescale (minutes to hours) and does not replace the existing low-level converter controls. While a typical MPC may directly set converter reference currents or duty cycle, the PSC alters only the rated power setting of each turbine system, acting as a supplementary system-level control action.

A. Overview

Following an MPC style framework, the PSC operates with a timestep T_S, a control horizon c, and a prediction horizon p, as shown in Fig. 8. Note that T_S is of the order of hours to days. The time at which the PSC process is called, denoted k, is measured from the beginning of the turbine array operation. Subsequent PSC process calls occur at $k + T_S$, $k + 2T_S$ and so on. At the end of the prediction horizon, the time is then $k + p$. The PSC implements peak-shaving by reducing the rated power of a turbine unit, causing it to enter the power-limited, variable-pitch region of operation at a slower speed than normal. The objective of the PSC is to minimize LCOE by obtaining the optimal set of rated powers, defined as the array $\boldsymbol{Prated_{opt}}$, corresponding to the lowest calculated LCOE at the end of the prediction horizon.

Fig. 9. shows a summary flowchart of the PSC process. Starting from the top, the PSC begins by defining an array of test rated powers $\boldsymbol{Prated_{test}}$ with length n_{points}, between the minimum forecasted power generation and turbine system base rated power $Prated_{base}$. The PSC process will simulate each turbine unit with each of the test rated powers over the prediction horizon. This yields the predicted system LCOE at the end of the prediction horizon for all possible combinations of test rated powers across the array. The simulation of each turbine unit for each test rated power is denoted "Subroutine A", and the LCOE calculations for the possible combinations across the array are denoted "Subroutine B", as explained next.

B. Subroutine A

The PSC process performs this subroutine, detailed in the blue shaded area of Fig. 9, for each turbine in the array and for each test rated power. e.g., for a three-turbine system, with ten values defined in the array $\boldsymbol{Prated_{test}}$, Subroutine A is performed $3 \times 10 = 30$ times. First, simulation of the turbine unit over the prediction horizon estimates the gen-side and grid-side PE converter IGBT temperatures and the turbine unit's energy generation. Next, these simulated temperatures are concatenated with the measured temperatures from time 0 to k to obtain temperature profiles from time 0 to p. Similarly, the turbine unit's simulated energy generation over the prediction horizon is summed with the measured energy at time k to give energy at time $k + p$. The PSC process then passes the temperature profiles to the lifetime models described in Section II. Therefore, for each turbine and test rated power, this Subroutine A outputs the predicted gen-side and grid-side converter LCs, and energy generation at time $k + p$.

C. Subroutine B

The PSC process performs this subroutine, detailed in the red shaded area of Fig. 9, for all combinations of test rated powers across the array. e.g., for a three-turbine system, with 10 test rated powers, Subroutine B is performed $10^3 = 1000$ times. As the PSC operates with T_S of order of hours, the computation time is not a concern for smaller turbine arrays. However, to deploy the PSC to large turbine arrays may require employing advanced computationally-efficient search algorithms or machine learning techniques. For example, in Subroutine A, a smaller set of test rated powers could be simulated, while in Subroutine B, combinations of test rated powers across the array could be more efficiently tested. As discussed in Section III, the turbine array uses a group CBM policy for the gen-side and grid-side converters. Therefore, the number of maintenance visits depends only on the gen-side and grid-side converters with the highest LC. Thus, the maximum gen-side and grid-side LCs are identified for the current combination of test rated powers. The number of maintenance visits per year to service the array's gen-side and grid-side converters is calculated as follows:

$$nvis/yr_{genside} = \frac{nvis_{genside} + max(\boldsymbol{LC_{genside}})}{(k+p)_{years}} \quad (25)$$

This article has been accepted for publication in IEEE Transactions on Energy Conversion. This is the author's version which has not been fully edited and content may change prior to final publication. Citation information: DOI 10.1109/TEC.2022.3231286

$$nvis/yr_{gridside} = \frac{nvis_{gridside} + max(\boldsymbol{LC_{gridside}})}{(k+p)_{years}} \quad (26)$$

where $nvis_{genside}$ and $nvis_{gridside}$ are the number of maintenance visits completed so far, until time k, for the gen-side and grid-side converters, $\boldsymbol{LC_{genside}}$ and $\boldsymbol{LC_{gridside}}$ are arrays of turbine unit gen-side and grid-side converter LCs across the array, and $(k+p)_{years}$ is the time at the end of the prediction horizon in years since the beginning of system operation. Note that the PSC considers non-integer values of maintenance visits per year.

At the end of the prediction horizon, the array energy generation is the summation of the turbine unit energies. Therefore, predicted annual energy production (AEP) is calculated as:

$$AEP = \frac{sum(\boldsymbol{E_{units}})}{(k+p)_{years}} \quad (27)$$

where $\boldsymbol{E_{units}}$ is the array of generated energies for each turbine unit. The variable OpEx cost per year is calculated as:

$$OpEx_{var} = (nvis/yr_{genside})(\$/visit_{genside}) + (nvis/yr_{gridside})(\$/visit_{gridside}) \quad (28)$$

where $\$/visit_{genside}$ and $\$/visit_{gridside}$ are the costs per visit for gen-side and grid-side converter group maintenance. Then the predicted LCOE at the end of the prediction horizon, for a given set of turbine units' test rated powers, is calculated as:

$$LCOE = \frac{FCR \cdot CapEx + OpEx_{fixed} + OpEx_{var}}{AEP} \quad (29)$$

where FCR is the fixed charge rate, $CapEx$ is the total capital costs, and $OpEx_{fixed}$ is the yearly fixed OpEx costs.

D. Optimal rated power selection

Following Subroutine B, the PSC has calculated the values of predicted LCOE for each combination of test rated powers across the turbine units in the array. The PSC then determines the optimal set of rated powers to apply to each turbine unit as the array $\boldsymbol{Prated_{opt}}$, as the combination of test rated powers that correspond to the minimum LCOE.

VI. PSC Simulation Case Study

Section IV showed that the peak-shaving actions central to the proposed PSC are potentially beneficial in a variable-speed, variable-pitch turbine system, but not in a variable-speed, fixed-pitch system. Therefore, this section now explores the potential benefit of the PSC to the example variable-pitch wind turbine array system, with the parameters in Tables I and II. Without direct access to full-power turbines and years of testing, a MATLAB simulation based case study provides valuable insights on the efficacy of the PSC.

The example array comprises three wind turbines, each of which exchanges measurements and rated power settings with the PSC as shown in Fig. 1. The case study uses a one-year-long wind velocity profile sampled at 5 minutes [26], shown in Fig. 10. Two test cases are defined. In case A, the wind speed observed at each turbine is identical (1x scaling from Fig. 10). In case B, the wind speed observed at T1 is scaled by 1.05x, at T2 by 1.00x, and at T3 by 0.95x. The disparity

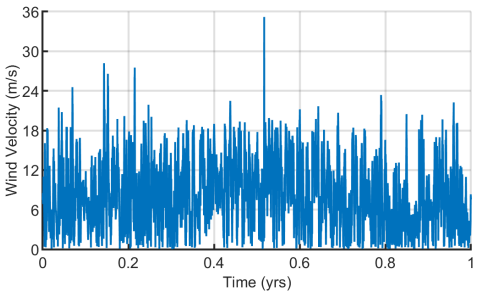

Fig. 10. One year wind velocity profile from [26].

in Case B wind speeds is used to investigate the behavior of the PSC when turbines across the array are aging at different rates, which can be realistic due to varying turbine placements and geography. Unless stated otherwise, the PSC uses an ideal forecast, where the wind forecast used by the PSC is identical to the experienced conditions. The case study compares the PSC results to baseline results where the turbine systems have fixed rated powers (PSC is not applied).

A. Determination of Economic Parameters

Performance of the PSC depends on the system's economic parameters. This subsection details how these parameters are set for the simulation case study. In reality, the economic parameters are set by the user according to the known or estimated costs of their specific system.

Firstly, a baseline simulation is performed for case A to obtain the AEP, $nvis/yr_{genside}$, and $nvis/yr_{gridside}$ without the PSC. Then we work backwards from baseline CapEx and OpEx values to obtain the required parameters for LCOE calculation using equations (25) through (29): $OpEx_{fixed}$, $\$/visit_{genside}$, and $\$/visit_{gridside}$. We define a constant CapEx value, unchanging across cases A and B, and between baseline and PSC simulations. Since the performance of the PSC is dependent on the relative balance of CapEx and OpEx costs, we consider performance over a range of "OpEx balance" values. We define "OpEx balance" as the OpEx share of the total LCOE costs, denoted as k_{OpEx}. For a given k_{OpEx} value, the total yearly OpEx cost for baseline case A is calculated as:

$$OpEx_{total} = \frac{k_{OpEx}}{1 - k_{OpEx}} \cdot FCR \cdot CapEx \quad (30)$$

The calculated $OpEx_{total}$ is then assumed to split evenly between fixed and variable OpEx costs, $OpEx_{fixed}$ and $OpEx_{var}$. This defines a set of $OpEx_{fixed}$ values changing only with k_{OpEx}. The cost per gen-side or grid-side converter maintenance visit is calculated from $OpEx_{var}$ as:

$$\$/visit_{genside} = \frac{OpEx_{var}}{nvis/yr_{genside} + nvis/yr_{gridside}} \quad (31)$$

$$\$/visit_{gridside} = \$/visit_{genside} \quad (32)$$

B. Wind Turbine Array

1) PSC Performance Compared to Baseline: LCOE is calculated after a one-year-long simulation of the wind turbine

This article has been accepted for publication in IEEE Transactions on Energy Conversion. This is the author's version which has not been fully edited and content may change prior to final publication. Citation information: DOI 10.1109/TEC.2022.3231286

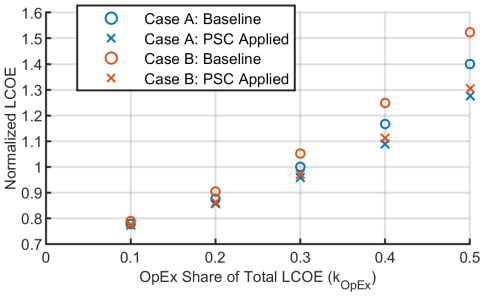

Fig. 11. Normalized LCOE results for various k_{OpEx} values.

array using equations (25) through (29). While the simulation is performed for one year only, the project lifespan is 12 years. However, this does not affect the LCOE calculation since the calculations use per-year values. Baseline and PSC system simulations are performed across test cases A and B, and at k_{OpEx} values of 10%, 20%, 30%, 40%, and 50%.

Fig. 11 shows the LCOE results normalized to the case A baseline simulation performed at k_{OpEx} = 0.3 (OpEx accounting for 30% of the total LCOE costs). Considering the baseline simulations, the changing k_{OpEx} value alters the $\$/visit_{genside}$ and $\$/visit_{gridside}$ values, leading to a changing LCOE across k_{OpEx}, despite constant energy generation and number of maintenance visits. Now considering the PSC results, changing k_{OpEx} also affects the behavior of the PSC process. At lower k_{OpEx} values, peak-shaving is less likely to reduce LCOE since the maintenance visit costs are lower. i.e., exchanging some energy generation for prolonged converter lifetimes becomes less tenable as the maintenance visit cost savings shrink. On the other hand, at higher k_{OpEx}, the trade-off becomes more advantageous since the maintenance visit costs are high. As mentioned in the introduction, $OpEx$ may not decrease as fast as $CapEx$ as turbine technologies mature; hence the proposed PSC will be more effective as k_{OpEx} increases.

Clearly from Fig. 11, the PSC reduces LCOE in cases A and B, across all k_{OpEx} values. Note that when $k_{OpEx} = 0.5$, the LCOE reduction can be as high as 14.3%. The larger LCOE reductions realized in case B are caused by the imbalanced wind speeds across the turbine array. In these cases, applying peak-shaving to one or two of the turbine units can reduce the group maintenance visits while only sacrificing energy generation in one or two turbine units. This condition arises from the group maintenance policy, in which only the gen-side or grid-side converter with the highest LC affects the scheduling of the maintenance visits.

2) Detailed Results for Case B and k_{OpEx} = 0.3: Fig. 12 shows the turbine units' energy production, gen-side converter LC, grid-side converter LC, and optimal rated powers for the baseline and PSC simulations. Energy and LCs are normalized to the final values for the baseline T2 turbine unit (1x wind speed scaling, no PSC). In the baseline case, the rated powers for all three turbines remain constant at 24 kW. In the PSC situation, the PSC process finds the optimal rated power for each turbine unit to minimize LCOE. The PSC process uses a timestep T_s of 3 hrs and a prediction horizon p of 24 hrs. The PSC significantly reduces T1 and T2 converter LCs compared

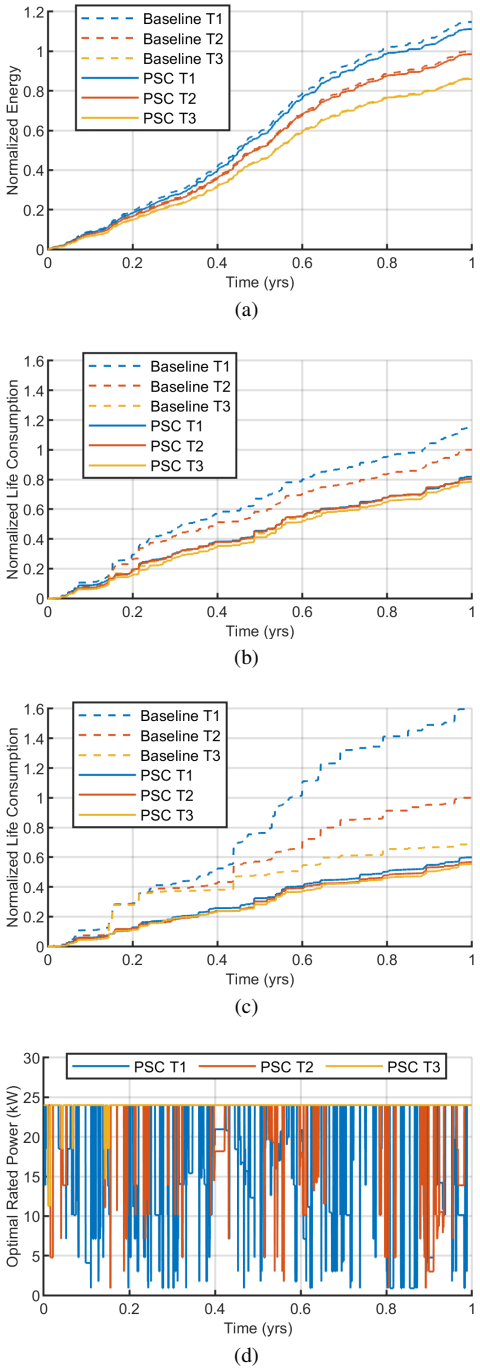

Fig. 12. Wind turbine array operation for baseline and PSC simulation cases over the one year profile of Fig. 10. (a) Normalized turbine unit energy generation. (b) Normalized gen-side converter LC. (c) Normalized grid-side converter LC. (d) Turbine unit optimal rated powers set by the PSC.

to the baseline, with only minor reductions in T1 and T2 energy generation. Under the group CBM policy described in Section III, the number of maintenance visits with the PSC applied is reduced compared to the baseline, leading to reduced $nvis/yr_{genside}$, $nvis/yr_{gridside}$, and $OpEx_{var}$. Since the PSC process minimizes LCOE in real-time, the PSC will always apply the optimal amount of peak-shaving considering the trade-off between energy generation and prolonged converter lifetimes.

This article has been accepted for publication in IEEE Transactions on Energy Conversion. This is the author's version which has not been fully edited and content may change prior to final publication. Citation information: DOI 10.1109/TEC.2022.3231286

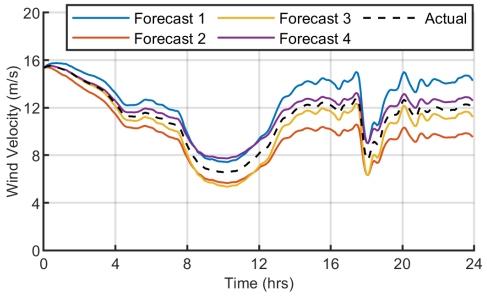

Fig. 13. Forecasts 1 through 4 compared to the actual wind velocity over a sampled 24 hr period of the Fig. 10 wind profile.

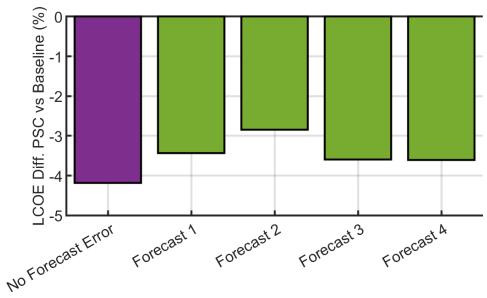

Fig. 14. LCOE with PSC compared to baseline (no PSC) for ideal forecast and forecasts 1 through 4. Results are for case A with $k_{opex} = 0.3$.

3) Effect of Forecasting Error: In the simulations presented so far, the PSC process has used an "ideal forecast" where the forecast exactly matches the observed wind speeds. A 24 hr forecast is used since the PSC prediction horizon p in the case study is 24 hrs long. Four synthesized forecasts are created from the actual wind velocities of Fig. 10, with an introduced mean average percentage error (MAPE) of zero at t = 0 hrs, rising to around 20 % at the forecast for +24 hrs, in line with typical forecast accuracies [27]. Fig. 13. shows the four synthesized forecasts compared to the observed wind velocity over an example 24 hr period.

The PSC is now simulated with each synthesized forecast for case A and k_{opex} = 0.3. Fig. 14 shows the LCOE reduction achieved by the PSC with the ideal forecast and forecasts 1 through 4, compared to the baseline case. The PSC achieves close to the ideal forecast scenario LCOE with all synthesized forecasts. In the worst scenario, LCOE is still reduced by 2.84% from the baseline.

We attribute the robustness of the proposed PSC to forecasting error to two factors. Firstly, in the MPC style framework of the PSC process, the step size is 3 hrs, and the prediction horizon is 24 hrs. Therefore, the PSC can often compensate for the large forecast errors encountered in the 12-24 hr ahead prediction period. Secondly, the PSC control variables are the turbine unit rated powers, meaning forecast absolute accuracy is not essential. Real-time minimization of LCOE dictates the peak-shaving actions, considering the trade-off between energy generation and PE converter aging due to thermal cycling. Thus, so long as the forecast approximately captures the amount of energy available and the number and magnitude of the swings in the wind or water velocity, forecasting error's impact on PSC performance remains limited.

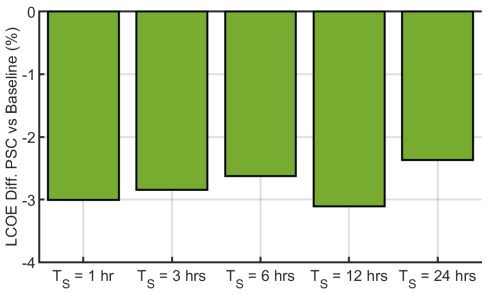

Fig. 15. LCOE with PSC compared to baseline for various timesteps T_S. Results are for simulation case A, k_{opex} = 0.3, and Forecast 2.

4) Effect of PSC Timestep: Here the effect of varying the PSC timestep is investigated. The results shown so far have all used a timestep T_S of 3 hrs. Now the PSC simulation for case A, Forecast 2, and k_{opex} = 0.3 is repeated with T_S values of 1, 6, 12, and 24 hrs. The LCOE results compared to the baseline are shown in Fig. 15. The largest LCOE reduction compared to the baseline is achieved with T_S = 12 hrs. At timesteps below 12 hrs, the differences are minimal and attributed to noise resulting from the discrete nature of the PSC test rated powers. At the higher T_S of 24 hrs, the error in the forecast begins to negatively impact PSC performance.

C. Discussion

While the presented results are promising - offering up to 14.3% LCOE reduction, they may be optimistic. One factor is that the economic model is simplistic in that it assumes maintenance visits account for half of the total $OpEx$ cost, and $OpEx$ accounts for a defined share of $CapEx$. Therefore, if the baseline simulation used to set the economic parameters returns a very low number of maintenance visits over the system lifespan, the model sets the cost of a single maintenance visit to be unrealistically high. Another factor is that the case study PE converters use a passive cooling system, in which the IGBTs are cooled via a heatsink on the nacelle / enclosure wall over which the wind flows. Research has shown that active cooling systems offer better cooling and longer device lifetimes than passive cooling systems [28]. Therefore, the PSC LCOE reduction in an actively cooled system may be smaller since the thermal cycle magnitudes may already be relatively small even before any peak-shaving is applied. Lastly, the lifetime models use extrapolation to extend the source data to additional temperature ranges, and the fundamental-frequency lifetime models use test data from a 2-second cycle test. In the lifetime test data, shorter cycle duration corresponds to reduced degradation. Therefore, treating each fundamental-frequency cycle identically to a 2-second cycle likely overestimates the degradation effects of these cycles.

VII. Conclusion

This paper proposed a PSC for reducing the LCOE of turbine array systems. Peak-shaving actions are implemented by varying the rated power of each turbine on-the-fly. The PSC process simulates the turbine array system over a prediction horizon, selecting the optimal rated powers for each turbine

unit by minimizing a function for predicted LCOE. Underlying the proposed PSC is the concept of exchanging energy generation for prolonged gen-side and grid-side converter lifetimes, which leads to reduced maintenance visits and OpEx costs. The PSC considers this trade-off in real-time by minimizing the LCOE at every PSC process timestep. In investigating the effect of peak-shaving, it was found that the PSC is most applicable to variable-speed variable-pitch turbines.

A hardware experiment demonstrated the impact of peak-shaving actions on the PE system. Then a simulation case study for an example variable-pitch wind turbine array investigated the PSC's impact on LCOE over the array's lifespan. Applying the proposed PSC was beneficial, reducing LCOE across various environmental and economic scenarios. The potential LCOE reduction increases with the share of LCOE attributed to OpEx costs. Further, larger LCOE reductions are realized in systems with unbalanced wind speeds across the turbine array. That said, the results appear optimistic compared to the LCOE reduction that may be observed in reality. Therefore, future work should improve the accuracy of the lifetime modeling, as well as employ a more comprehensive economic model of the turbine system. Further, should the variable-pitch technology become mature in the HKT sector, the proposed PSC framework will still apply.

This work offers several contributions. First the proposed PSC expands the concept of power control for improved system economics to a turbine array using a group CBM strategy. Further, altering the rated power of each turbine unit on-the-fly (derating) is demonstrated as an effective means of implementing power control via distinct peak-shaving actions. Setting the rated power allows PSC implementation without altering the existing turbine unit controls. Using turbine rated power as the control variable also allows the PSC to operate with a slow timescale and robustness to absolute errors in the forecasted wind or water speeds. Finally, minimizing the predicted LCOE function in real-time as part of the PSC process ensures the PSC will optimize system economics throughout the system lifetime. Therefore, the proposed PSC offers a valuable tool for further optimizing future turbine array systems.

REFERENCES

[1] R. Wiser, M. Bolinger, B. Hoen, D. Millstein, J. Rand, G. Barbose, N. Darghouth, W. Gorman, S. Jeong, A. Mills, and B. Paulos, "Land-Based Wind Market Report: 2021 Edition," p. 87.

[2] C. M. Niebuhr, M. van Dijk, V. S. Neary, and J. N. Bhagwan, "A review of hydrokinetic turbines and enhancement techniques for canal installations: Technology, applicability and potential," *Renewable and Sustainable Energy Reviews*, vol. 113, p. 109240, Oct. 2019.

[3] C. Röckmann, S. Lagerveld, and J. Stavenuiter, "Operation and Maintenance Costs of Offshore Wind Farms and Potential Multi-use Platforms in the Dutch North Sea," in *Aquaculture Perspective of Multi-Use Sites in the Open Ocean: The Untapped Potential for Marine Resources in the Anthropocene*, B. H. Buck and R. Langan, Eds. Cham: Springer International Publishing, 2017, pp. 97–113.

[4] T. Stehly and P. Duffy, "2020 Cost of Wind Energy Review," NREL, Tech. Rep. NREL/TP-5000-81209, Dec. 2021. [Online]. Available: https://www.osti.gov/biblio/1838135-cost-wind-energy-review

[5] R. Wiser, M. Bolinger, and E. Lantz, "Assessing wind power operating costs in the United States: Results from a survey of wind industry experts," *Renewable Energy Focus*, vol. 30, pp. 46–57, Sep. 2019.

[6] A. D. Riva, J. Hethey, S. Luers, A.-K. Wallasch, K. Rehfeldt, A. Duffy, D. E. Weir, M. Stenkvist, A. Uihlein, T. J. Stehly, E. Lantz, and R. Wiser, "IEA Wind TCP Task 26: Wind Technology, Cost, and Performance Trends in Denmark, Germany, Ireland, Norway, Sweden, the European Union, and the United States: 2008-2016," NREL, Tech. Rep. NREL/TP-6A20-71844, Jun. 2019. [Online]. Available: https://www.osti.gov/biblio/1525772

[7] K. L. Dykes, M. M. Hand, E. J. Lantz, T. J. Stehly, M. C. Robinson, P. S. Veers, and R. Tusing, "Enabling the SMART Wind Power Plant of the Future Through Science-Based Innovation," NREL, Tech. Rep. NREL/TP-5000-68123, Aug. 2017. [Online]. Available: https://www.osti.gov/biblio/1378902

[8] M. Previsic, "The Future Potential of Wave Power in the United States," RE Vision Consulting, Tech. Rep., Aug. 2012.

[9] G. Rinaldi, P. R. Thies, and L. Johanning, "Current Status and Future Trends in the Operation and Maintenance of Offshore Wind Turbines: A Review," *Energies*, vol. 14, no. 9, 2484, Jan. 2021.

[10] F. Camci, "System Maintenance Scheduling With Prognostics Information Using Genetic Algorithm," *IEEE Trans. Rel.*, vol. 58, no. 3, pp. 539–552, Sep. 2009.

[11] F. Besnard, M. Patriksson, A.-B. Strömberg, A. Wojciechowski, and L. Bertling, "An optimization framework for opportunistic maintenance of offshore wind power system," in *IEEE Bucharest PowerTech*, Jun. 2009, pp. 1–7.

[12] E. Pazouki, H. Bahrami, and S. Choi, "Condition Based Maintenance optimization of wind turbine system using degradation prediction," in *IEEE PES General Meeting | Conf. Expo.*, Jul. 2014, pp. 1–5.

[13] M. Shafiee, "An optimal group maintenance policy for multi-unit offshore wind turbines located in remote areas," in *Int. Conf. on Probabilistic Methods Applied to Power Systems*, Jul. 2014, pp. 1–6.

[14] Y. Chen, L. Wang, S. Liu, and G. Wang, "A Health-oriented Power Control Strategy of Direct Drive Wind Turbine," *IEEE Trans. Power Del.*, vol. 37, no. 2, pp. 1324–1335, 2022.

[15] B. Whitby and C. E. Ugalde-Loo, "Performance of Pitch and Stall Regulated Tidal Stream Turbines," *IEEE Transactions on Sustainable Energy*, vol. 5, no. 1, pp. 64–72, Jan. 2014.

[16] F. D. Bianchi, H. De Battista, and R. J. Mantz, *Wind turbine control systems: principles, modelling and gain scheduling design*, ser. Advances in industrial control. London: Springer, 2007.

[17] D. Graovac, M. Purschel, and A. Kiep, *MOSFET Power Losses Calculation Using the Data-Sheet Parameters*, App. Note, Infineon, 2006.

[18] J. G. H. an G. A. Goodarzi, *Electric Powertrain: Energy Systems, Power Electronics and Drives for Hybrid, Electric and Fuel Cell Vehicles*. John Wiley & Sons, Ltd, 2017.

[19] *Standard Practices for Cycle Counting in Fatigue Analysis*, ASTM International Std. ASTM E1049-85(2017), 2017.

[20] L. Wang, J. Xu, G. Wang, and Z. Zhang, "Lifetime estimation of IGBT modules for MMC-HVDC application," *Microelectronics Reliability*, vol. 82, pp. 90–99, Mar. 2018.

[21] *IKW20N60T*, Datasheet, Infineon, 2015. [Online]. Available: https://www.infineon.com/dgdl/Infineon-IKW20N60T-DS-v02_08-EN.pdf?fileId=5546d4624f205c9a014f20e3e11900ef

[22] M. Pecht and A. Dasgupta, "Physics-of-failure: an approach to reliable product development," in *IEEE 1995 Int. Integrated Reliability Workshop. Final Report*, Oct. 1995, pp. 1–4.

[23] H. Wang, M. Liserre, F. Blaabjerg, P. de Place Rimmen, J. B. Jacobsen, T. Kvisgaard, and J. Landkildehus, "Transitioning to Physics-of-Failure as a Reliability Driver in Power Electronics," *IEEE Trans. Emerg. Sel. Topics Power Electron.*, vol. 2, no. 1, pp. 97–114, Mar. 2014.

[24] E. Özkol and S. Hartmann, *Load-cycle Capability of HiPak IGBT Modules*, Application Note 5SYA 2043-04, Hitachi Energy,, 2022.

[25] M. Musallam, C. Yin, C. Bailey, and M. Johnson, "Mission Profile-Based Reliability Design and Real-Time Life Consumption Estimation in Power Electronics," *IEEE Trans. Power Electron.*, vol. 30, no. 5, pp. 2601–2613, May 2015.

[26] Western wind data set. NREL. [Online]. Available: https://www.nrel.gov/grid/western-wind-data.html

[27] I. Okumus and A. Dinler, "Current status of wind energy forecasting and a hybrid method for hourly predictions," *Energy Conversion and Management*, vol. 123, pp. 362–371, Sep. 2016.

[28] F. Wani, U. Shipurkar, J. Dong, H. Polinder, A. Jarquin-Laguna, K. Mostafa, and G. Lavidas, "Lifetime analysis of igbt power modules in passively cooled tidal turbine converters," *Energies*, vol. 13, no. 8, 1875, 2020.

Alastair P. Thurlbeck (Member, IEEE) received the M.Eng. degree (first class honors) in electronics and electrical engineering from the University of Glasgow, Glasgow, UK, in 2018, and Ph.D. degree in electrical and computer engineering from Oregon State University (OSU), Corvallis, OR, USA, in 2022.

Mr. Thurlbeck is currently a Researcher with the Electric Vehicle Grid Integration team at the National Renewable Energy Laboratory (NREL), Golden, CO, USA. He has been a Research Scientist Intern at Amazon Prime Air in Seattle, WA, USA; a Project Assistant with the University of Glasgow; and a Hardware Intern with Curtis Instruments in Livermore, CA, USA.

Mr. Thurlbeck received the IEEE ITEC Conference Student Award in 2019. He was awarded the Gilbert Cook Prize in 2018, the William Dawson Bursary in 2015 and the Reid Foster prize in 2014 by the University of Glasgow. He was a recipient of the Diamond Jubilee Scholarship throughout his MEng degree, awarded by the Institute of Engineering and Technology (IET) in 2013.

Yue Cao (Senior Member, IEEE) received the B.S. degree (Hons.) in electrical engineering with a second major in mathematics from the University of Tennessee, Knoxville, TN, USA, in 2011, and the M.S. and Ph.D. degrees in electrical engineering from the University of Illinois at Urbana–Champaign (UIUC), Champaign, IL, USA, in 2013 and 2017, respectively.

Dr. Cao is currently an Assistant Professor with the Energy Systems Group at Oregon State University (OSU), Corvallis, OR, USA. Before joining OSU, he was a Research Scientist with the Propulsions Team at Amazon Prime Air in Seattle, WA, USA. He was a Power Electronics Engineer Intern with Special Projects Group at Apple Inc., Cupertino, CA, USA; Halliburton Company, Houston, TX, USA; and Oak Ridge National Laboratory, TN, USA. He was a Sundaram Seshu Fellow in 2016 at UIUC, where he was a James M. Henderson Fellow in 2012. His research interests include power electronics, motor drives, and energy storage with applications in renewable energy integration and transportation electrification.

Dr. Cao was a national finalist of the USA Mathematical Olympiad (USAMO) in 2006 and 2007. He received the Myron Zucker Student Award from the IEEE Industry Applications Society (IAS) in 2010. He won the Oregon State Learning Innovation Award for transformative education in 2020. He is a recipient of the 2022 NSF CAREER award. He is selected into U.S. National Academy of Engineering (NAE) Frontiers of Engineering (FOE) Class of 2022. Dr. Cao was the Special Sessions Chair of the 2022 IEEE Energy Conversion Congress Expo (ECCE) and the Tutorials Chair of 2021 ECCE. He is a board member and Award Chair of IEEE Power Electronics Society (PELS) TC11 – Aerospace Power. In 2020, he helped establish an IEEE PELS Chapter at OSU. He is currently an Associate Editor for IEEE Transactions on Transportation Electrification and an Associate Editor for IEEE Transactions on Industry Applications.